Heliyon 12 (2026) e44621

Contents lists available at ScienceDirect

Heliyon

journal homepage: www.cell.com/heliyon

Research article

Subtle blood-brain barrier leakage quantification using DCE-MRI in subjective and mild cognitive impairment: A pilot sub-study of the Cognitive Ageing, Nutrition & Neurogenesis (CANN) trial

Rashed Sobhan [a,b], Michael J. Thrippleton [c], David R. Willis [a], Rachel Gillings [a], Saber Sami [a], Joanna M. Wardlaw [c], Anne-Marie Minihane [a], Narelle M. Berry [a,1,2], Donnie Cameron [a,d,*,1]

[a] Norwich Medical School, University of East Anglia, Norwich, United Kingdom
[b] Sir Peter Mansfield Imaging Centre, University of Nottingham, United Kingdom
[c] Centre for Clinical Brain Sciences, University of Edinburgh, United Kingdom
[d] Department of Medical Imaging, Radboud University Medical Center, Nijmegen, the Netherlands

ARTICLE INFO

Keywords:
Blood-brain barrier
Mild cognitive impairment
Subjective memory impairment
Permeability
Dietary supplement
T_1 mapping

ABSTRACT

The pathophysiology of dementia relates to leakage of the aging blood-brain barrier (BBB). Dynamic contrast-enhanced (DCE)-MRI quantifies this leakage and may facilitate early diagnosis and treatment monitoring. Here, we present preliminary work comparing BBB leakage and T_1 between mild and subjective cognitive impairment (MCI and SCI) participants (n = 6 and 17, respectively) after year-long consumption of a *combined* omega-3 fatty acid (fish oil capsules) and cocoa flavanol-3-ol (chocolate drops) dietary supplement or matched-control (n = 1/5 MCI and 9/8 SCI). DCE-MRI data from white matter, grey matter, hippocampus, thalamus, and amygdala were fitted with the Patlak model to obtain the permeability-surface-area product (PS), and pre-contrast T_1 was calculated. No differences were observed between intervention groups. After combining control and active groups, we observed greater leakage (PS) in the MCI hippocampus (p = 0.019) and thalamus (p = 0.042) versus SCI, and longer T_1 values in MCI white matter (p = 0.042) and thalamus (p = 0.023). This preliminary study indicates the potential utility of BBB leakage and T_1 in differentiating MCI and SCI. This should be investigated further in larger trials.

1. Introduction

The blood-brain barrier (BBB) plays an important role in separating the parenchyma of the central nervous system from the blood [1]. It allows the passage of oxygen, carbon dioxide, water, and essential nutrients, and prevents the movement of harmful substances (e.g., harmful bacteria, toxins) into brain tissue. Leakage in the BBB's tightly-packed layers of endothelial cells is indicative of aging and pathologies such as vascular dementia, Alzheimer's disease, and cerebral small vessel disease [2,3], as has recently been

* Corresponding author. Department of Medical Imaging (Route 766), Radboud University Medical Center, Geert Grooteplein 10, PO box 9101, 6500 HB, Nijmegen, the Netherlands.
E-mail address: donnie.cameron@radboudumc.nl (D. Cameron).
[1] Narelle Berry and Donnie Cameron contributed equally to this work.
[2] Narelle Berry passed away on the 24th of July 2019.

https://doi.org/10.1016/j.heliyon.2026.e44621
Received 8 July 2024; Received in revised form 6 February 2026; Accepted 11 February 2026
Available online 18 February 2026

Abbreviations

AIF	Arterial input function
CANN	Cognitive Ageing, Nutrition, and Neurogenesis
DCE	Dynamic contrast enhanced
DESPOT1-HIFI	Driven Equilibrium Single Pulse Observation T1 with High-speed Incorporation of RF Field Inhomogeneities
GBCA	Gadolinium-based contrast agent
PS	Permeability-surface area product
SCI	Subjective cognitive impairment
SPGR	Spoiled gradient-recalled echo
VIF	Vascular input function

highlighted in animal models [4,5]. Early detection of BBB damage could serve not only to predict the onset of these diseases, but also to develop interventions that can delay their progress [6,7]. One of the early stages of the cognitive decline due to Alzheimer's disease and vascular dementia is termed mild cognitive impairment (MCI). This condition is characterized by further worsening of BBB integrity on top of the increased leakage associated with healthy aging [8–10]. Another phenotype, termed subjective cognitive impairment (SCI) or subjective memory impairment, has been proposed by some as the first clinical manifestation of Alzheimer's disease [11]. This self-diagnosed condition is associated with subjective complaints of cognitive functioning, without evidence of objective cognitive impairment. Quantitative measurement of microvascular integrity could not only assist in the diagnosis, treatment planning, and monitoring of the neuropathological progression of SCI and MCI, but could also be used to establish the effectiveness of any therapeutic or dietary interventions that aim to mitigate age- or pathology-associated BBB dysfunction and neurocognitive decline.

In aging and pre-dementia populations, dietary bioactive intake and dietary patterns have been associated with memory, cognition, and potential effects on cerebral blood flow [12–17]. Dietary changes may therefore reduce the risk, delay the onset, or slow the pathology of dementia. Data from observational studies on healthy groups and those with existing cognitive deficits have reported mixed findings for the effects of fish-derived long chain omega-3 intake on decreasing the risk of Alzheimer's disease, dementia, and cognitive decline [18–21]. Moreover, many studies suggest that intake of specific flavonoids—naturally occurring polyphenolic compounds found in plant-based foods, such as teas, cocoa and berries [22]—is linked to improved cognitive function and reduced risk from age-related neurodegenerative diseases [23,24]. Although individual efficacy of omega-3 or flavonoids has been investigated, their combined impact on cognition or cerebral vasculature had not been explored until the recent Cognitive Ageing, Nutrition, and Neurogenesis (CANN) trial [25,26].

MRI presents an ideal, high-tissue-contrast, non-ionizing modality for quantitative measurement of microvascular integrity and for exploring the effects of dietary interventions thereon. The most widely used quantitative method to measure BBB integrity is dynamic contrast-enhanced (DCE) MRI. This imaging technique involves injecting an exogenous Gadolinium-based contrast agent (GBCA) and acquiring T_1-weighted MR images before, during, and after injection. Aging, dementia, and cerebral small vessel diseases are all associated with BBB damage, which leads to leakage of GBCA from plasma to the extravascular extracellular space—shortening the longitudinal relaxation time constant and increasing the corresponding signal intensity on T_1-weighted DCE-MRI.

Quantitative analysis of DCE-MRI involves fitting of pharmacokinetic models to signal enhancement curves and obtaining certain target parameters: the fractional plasma volume (v_p), fractional interstitial volume (v_e), plasma flow (F_p), permeability-surface area product (PS), and volume transfer constant (K^{trans}) [27]. Due to subtle leakage of GBCA in MCI and SCI cohorts, post-contrast DCE-MRI enhancement is relatively small compared to the pronounced BBB permeability associated with high grade tumors, infarction, acute multiple sclerosis lesions, and acute inflammation [10,28,29], approaching 5% in grey matter (GM) and 1−2% in white matter (WM). Although several studies have explored permeability for MCI and normal older subjects for multiple brain regions such as white matter [30], normal-appearing white matter, white matter hyperintensities, deep and cortical grey matter [1,9], the hippocampus [8], and different sub-regions of white matter and cortical and deep grey matter [31,32], no study, to our knowledge, has compared DCE-parameters between cohorts with MCI and SCI in order to assess the suitability of DCE-MRI for characterizing the progression of the neuropathology and associated cognitive decline. Moreover, the existing studies have demonstrated substantial variability in analysis and the resultant parameter estimates [10]. Accurate permeability quantification demands a processing pipeline that conforms to consensus recommendations [7], addressing systematic errors arising from issues like scanner drift, RF field inhomogeneity, and fast or slow water exchange assumptions for longitudinal relaxation modeling.

In this pilot study, we compare MCI and SCI groups in terms of BBB integrity, incorporating recent advancements in DCE-MRI analysis. Initially, in a small cohort, we quantify BBB leakage for larger brain regions (WM and GM) and in subcortical regions involved in memory processing. Also, group analysis is performed to explore differences in cortical thickness and segmentation volumes between SCI and MCI cohorts. Finally, as a sub-study of the CANN trial [25], we perform a preliminary assessment of the effectiveness of a *combined* dietary intervention in improving microvascular integrity. Our hypotheses are: first, BBB leakage differs between MCI and SCI cohorts; and second, BBB leakage is lower in both groups after intervention with *combined* omega-3 fatty acids and flavonoids.

2. Materials and methods

2.1. Participants and dietary intervention

This study was conducted as an adjunct pilot investigation of the CANN study: a randomized-controlled trial run by the University of East Anglia, Norwich, UK, and Swinburne University of Technology, Melbourne, Australia between August 2015 and March 2018. The purpose of CANN was to investigate the efficacy of a *combined* omega-3 fatty acid and flavanol (flavonoids derived from cocoa) intervention termed OM3FLAV on cognitive performance, brain structure and blood flow, systemic vascular function, circulating biomarkers of inflammation and brain function, and microflora composition and metabolism in older adults with MCI or SCI. Ethical approval in the UK was granted by the National Research Ethics Service Committee (Study ID: 14/EE/0189) including a substantial amendment in May 2017 to permit the addition of DCE-MRI. The parent trial was registered on clinicaltrials.gov (NCT02525198). Inclusion criteria were: age between 55 and 84 years; no history of smoking; no history of diabetes mellitus; no indication of a clinically-diagnosed psychiatric disorder; no history of familial monogenic form of cognitive decline; and no allergies to fish or any other component in the intervention supplements. Participants with uncontrolled hypertension and BMI $\geq$40 kg/m^2 were excluded. Detailed inclusion and exclusion criteria in relation to medications, life-style status, dietary status, MRI contraindications, etc. can be found in Irvine et al., 2018 [25]. Participants were recruited in the vicinity of Norwich, UK, via general practitioner surgeries, general advertising, newspaper articles, and radio programs. Each participant received a comprehensive description of the study, including possible risks, and gave written informed consent prior to participation.

Participants were classed as MCI based on criteria developed by the National Institute on Aging—Alzheimer's Association workgroup [33]: the participant is concerned about worsening of their memory in the last two−to−three years, their functional abilities are preserved, and they are not demented or depressed. Participants were classified as SCI when they met all these criteria but scored less than one standard deviation below the mean on all measures in the MCI neuropsychological battery: namely, their score was in the normal range for their age and education, but there were significant concerns regarding memory worsening.

At the CANN trial's UK site, a total of 17 SCI and 6 MCI subjects consented to participate in this DCE-MRI sub-study between May and November 2017. Of these participants, 10 underwent the full CANN imaging protocol—which included arterial spin labeling MRI, functional MRI, diffusion tensor MRI, and ^{1}H MR spectroscopy—while the remaining 13, who were left-handed and were thus ineligible for the full protocol, underwent a truncated protocol comprising structural imaging and DCE-MRI only.

MCI and SCI subjects were split into further groups based on their participation in the two intervention arms of the parent CANN trial. The active intervention group consumed the OM3FLAV (orally, each day for one year) as fatty-acid containing fish oil capsules (1.5 g of the marine omega-3 fatty acids; 0.4 g eicosapentaenoic acid, EPA; and 1.1. g docosahexaenoic acid, DHA) and 550 mg of cocoa flavan-3-ols as chocolate drops. The control group consumed flavanol-poor chocolate drops and omega-3-free oil control capsules. Thus, participants were categorized into four sub-groups: SCI with dietary intervention (SCI-active, SCI-a), SCI with control intervention (SCI-control, SCI-c), MCI with dietary intervention (MCI-active, MCI-a), and MCI with control intervention (MCI-control, MCI-c).

2.2. MRI acquisition

All MRI scans were performed according to the timeline of the parent CANN trial, coinciding with 12 months of dietary intervention. Scans were acquired using a 70-cm-bore 3T scanner (Discovery 750w; GE Healthcare, Milwaukee, WI, USA) with a 12-channel head coil for reception. Our 30-min truncated DCE-MRI protocol included the following sequences.

- 3D T_1-weighted inversion-recovery-(IR)-prepared fast spoiled gradient-recalled echo (SPGR) with TR = 7.2 ms and TE = 2.6 ms, section thickness = 1 mm, matrix = 256 × 256, and field of view (FoV) = 230 mm × 230 mm.
- 3D Driven Equilibrium Single Pulse Observation T_1 with High-speed Incorporation of RF Field Inhomogeneities (DESPOT1-HIFI) experiment comprising SPGR acquisitions with flip angles (FAs) of 5, 10, and 15°, and an IR-SPGR acquisition with an FA of 5° and a TI of 450 ms. Other parameters were as follows: TR/TE = 5.6/1.6 ms, FoV = 240 mm × 240 mm, section thickness = 4 mm, matrix = 144 × 144. The IR-SPGR scan was acquired with double the section thickness in the L-R direction.
- A 10.5-min 3D multi-phase SPGR sequence (FA = 15°, matrix = 144 × 96, temporal resolution = 31 s, TR/TE = 6.3/2.4 ms) with geometry matching the DESPOT1-HIFI was run after injection of GBCA (Gadovist®, Bayer Healthcare AG, Berlin, Germany) at a dose of 0.1 mmol/kg body weight and a rate of 1 ml/s.

To assess scanner drift, an identical protocol was run in seven age- and BMI-matched healthy volunteers with no GBCA injection.

2.3. Data pre-processing and analysis

2.3.1. Brain segmentation

Brain extraction and head-motion correction of DCE-MRI data was performed using the 'BET' and 'MCFLIRT' tools, respectively, from the FMRIB Software Library (FSL) [34,35]. The structural T_1-weighted images and motion-corrected DCE-MRI data were aligned to the 15°-SPGR images using the rigid-body registration tool 'FSL-FLIRT' [34,36]. Finally, FastSurfer (a deep-learning-based version of FreeSurfer) [33] was used to segment the structural data into two larger brain regions—WM and GM—and three subcortical regions typically involved in memory processing and storage: the hippocampus, thalamus, and amygdala.

2.3.2. Parametric maps

Further analysis was performed using pipelines developed in Python (version 3.9.1). The DESPOT1-HIFI method, comprising one IR-SPGR and three DESPOT1-SPGR acquisitions, was used to measure pre-contrast T_1 with voxel-wise correction for RF field (B_1^+) variation. Correction for B_1^+ was necessary as magnetic field inhomogeneities cause the transmitted flip angle (α_T) to be different from the prescribed FA (α_p) set by the scanner. A linear relationship between α_T and α_p, namely, $\alpha_T = \kappa\alpha_p$, was assumed, where κ is the relative FA, which accounts for the spatial variation of the B_1^+ field. As previously described [10,37], the DESPOT1-HIFI data for each voxel were fitted to obtain spatial maps for three free parameters: relative FA (κ), pre-contrast T_1, and proton density, based on the methods of Deoni et al. and Deichmann et al. [38,39].

2.3.3. Signal drift analysis

Prior to further analysis of signal intensities, the effect of signal drift was assessed using the sham DCE-MRI data. Signal intensities of each ROI were normalized by dividing the signal at each time point by the signal intensity averaged over the ROI. Signal drift in each subject was measured as the slope of a linear fit to these normalized signal intensities per ROI. Then, the mean and standard deviation of the drift over all subjects were calculated per ROI. Based on analyses performed by Armitage et al., we disregarded the effect of signal drift in our analyses if the mean drift was within one standard deviation of the signal enhancement equivalent to the change of one signal unit ($1/S_0$), where S_0 is the baseline signal [29].

2.3.4. Signal enhancement and dynamic concentration estimation

For each ROI, the median signal intensity (S_i) over all voxels was calculated for each time point *i*. The signal enhancement E_i was then calculated as $E_i = \frac{S_i - S_0}{S_0}$, where S_0 is the baseline signal intensity of the pre-contrast acquisition (with flip angle $\alpha_p = 15°$). From these signal enhancement curves, concentration time curves were estimated analytically using the SPGR signal equation [40], assuming a linear relationship between the longitudinal relaxation rate, R_1, and concentration, that is $C(t)$: $R_1 = R_{1o} + r_1 C(t)$; where R_{1o} is the longitudinal relaxation rate with contrast and r_1 (=5.0 mM^{-1} s^{-1}) is the proportionality constant, i.e. relaxivity [41].

2.3.5. Pharmacokinetic modeling

For pharmacokinetic modeling of the concentration time curves, the Patlak model was used, as suggested by several published studies [10,28,37]. This model has two key assumptions: negligible GBCA back flux and high perfusion relative to leakage. These assumptions are satisfied for acquisitions with lower temporal resolution and pathologies with subtle BBB disruption. Moreover, the use of this model provides a satisfactory compromise between model complexity and goodness of fit [28]. In the Patlak model, the concentration of GBCA is given by:

$$C_t(t) = v_p C_p(t) + PS \int_0^t C_p(\tau) d\tau \quad (1)$$

Here, $C_p(t)$ is the concentration of GBCA in plasma; v_p is the plasma volume, and PS is the permeability surface area product, which is equivalent to the volume transfer constant (K^{trans}) in the slow indicator exchange limit (where perfusion is much higher than leakage).

A vascular input function (VIF) was used as a surrogate for measurements of $C_p(t)$ in Equation (1). This VIF was manually determined from a voxel located in the superior sagittal sinus (SSS). VIFs are less affected by partial volume effects, and the delay between plasma concentration and VIF is small relative to the temporal resolution [27,28]. For conversion from VIF enhancement to concentration, the pre-contrast T_1 and relative FA values for the SSS voxel were taken from each subject's already-calculated native T_1-and relative-FA-maps. This determined the whole-blood concentration time course, $C_b(t)$, which was then converted to plasma concentration $C_p(t)$ using: $C_p(t) = \frac{C_b(t)}{1 - Hct}$, where Hct is the hematocrit measurement obtained for each subject from their recent clinical record. During Patlak model fitting, the first four data points (amounting to a period of 124 s) were ignored to exclude first-pass and early-post-injection effects, as prescribed by several published studies [28,42].

2.3.6. Permeability extraction and cortical thickness analysis

The Patlak model was fitted to dynamic concentration curves per subject using an unconstrained multiple linear regression approach and estimates for v_p and PS were extracted, as markers of plasma volume and BBB permeability, respectively. Finally, we calculated subcortical volumes and cortical parcellation thicknesses for each FreeSurfer-extracted ROI for all groups.

2.4. Statistical analysis

All statistical analyses on permeability parameters (PS and v_p) and pre-contrast T_1 were performed in MATLAB (v2020b, Mathworks, Natick, MA, USA). For each ROI, we compared group-wise differences in PS, v_p, and pre-contrast T_1 between cohorts using the Wilcoxon rank sum test for non-parametric data with a Bonferroni-corrected significance value, $p = 0.016$. Group differences in cortical thickness and segmentation volume were measured using a general linear model (GLM), with cluster-wise correction for multiple comparisons applied on the group-level contrast maps by running a permutation simulation with 1000 iterations, a cluster-forming threshold of 4, and a cluster-wise threshold of 0.05, adjusted for two hemispheres. Finally, to improve the statistical power, we ultimately merged the MCI and SCI subgroups under the assumption that the intervention does not affect the sub-groups, as concluded from the parent CANN study [22,23]. For this comparison of v_p, PS, and T_1, only two groups were studied (namely, SCI-a+c vs.

MCI-a+c); therefore, Bonferroni correction for multiple comparisons was not used ($p = 0.05$).

3. Results

3.1. Participant demographics

Table 1 shows the participant demographics, including blood pressure, education, Montreal Cognitive Assessment (MoCA) scores, and *APOE* ε4 carrier status. All *APOE* ε4 carriers were *APOE* ε4 heterozygous. We included 23 participants (16 Male) with mean [range] age of 67 [56−81] yrs. Given that this investigation was run as an adjunct sub-study during the original CANN trial, we were blinded to each participant's intervention group. After unblinding, it was revealed that 9 SCI subjects and 1 MCI were in the group who consumed OM3FLAV, whereas 8 SCI and 5 MCI participants received the control intervention. The MCI-a group ($n = 1$) was only included in the statistical analysis comparing the combined SCI (SCI-a+c) and MCI (MCI-a+c) groups, and is shown elsewhere, in figures and tables, only for completeness.

3.2. Segmentation and parametric maps

Fig. 1(a) shows the segmentation results from one SCI participant who underwent the OM3FLAV intervention (i.e., SCI-active). The native T_1, relative FA (κ), and proton density map for the participant is shown in Fig. 1(b). The subcortical regions were well-segmented with FastSurfer. The native T_1 map also shows good agreement with typical longitudinal relaxation time constants for different brain regions in healthy subjects.

The relative FA tended to be higher than 1 across most of the brain, which supports the established knowledge that the α_T often differs from the nominal FA, α_p, set by the scanner for 3T or higher field strengths [10,28,37]. Given that DESPOT1 is very sensitive to B_1^+ field inhomogeneity, any DCE-MRI acquisition and processing pipeline should incorporate B_1^+ correction.

3.3. Scanner drift was not significant

Fig. 2 presents the drift in median signal enhancement for each ROI for non-contrast data. The mean and standard deviation of one signal unit (i.e. $1/S_0$) were: WM: 0.06 (0.9), GM: 0.09 (1.0), hippocampus: 0.11 (1.0), thalamus: 0.08 (0.8), amygdala: 0.11 (1.1), as percentage enhancement at one time point: baseline. The mean and standard deviation of the slope of the relative enhancement curves (in units of percentage enhancement per second) for each ROI over all subjects were as follows: WM = 0.05 (0.21), GM = 0.05 (0.23), hippocampus = 0.12 (0.54), thalamus = 0.12 (0.31), amygdala = 0.08 (0.81), with all slopes showing a small positive trend. So, for all ROIs, the average drifts were within one standard deviation of a single signal unit ($1/S_0$). Consequently, the effect of signal drift was not considered for the rest of the analyses, as per the criteria suggested by Armitage et al. [26].

3.4. Permeability and native T_1 did not differ between SCI and MCI intervention sub-groups

The average signal enhancement per ROI is shown in Fig. 3 for all cohorts. The concentration time courses and their Patlak fits are shown in Fig. 4(a–b) for two subjects: one from the SCI-active group, for whom example images are also shown in Fig. 1, and another from the MCI-control group.

Table 2 shows the median and inter-quartile range (IQR) for v_p and PS, and Fig. 5 shows boxplots of these DCE-parameters, with the single MCI-active participant shown for reference. No significant differences were observed in v_p, PS,or T_1 between any of the three $n > 1$ groups ($p > 0.016$).

For larger regions like the WM and GM, the IQRs of the DCE parameters and T_1 values of the groups overlapped. For subcortical regions involved in memory processing, there was an increasing, non-significant trend in the leakage (PS) for the MCI cohort, and T_1

Table 1
Participant demographics for each of the three studied cohorts and one MCI-active subject[a].

Demographics	Total Cohort ($n = 23$)	SCI-control ($n = 8$)	SCI-active ($n = 9$)	MCI-control ($n = 5$)	MCI-active ($n = 1$)
Mean (SD) age, yrs	66.5 (13.8)	64.3 (9.9)	70.3 (11.8)	69.2 (14.7)	68.9
Sex, *n* (%) male	16 (69.6)	5 (62.5)	7 (77.8)	3 (60)	1 (100)
BMI, kg/m^2	26.1 [4.1]	26.9 [2.9]	24.4 [4.5]	26.2 [3.5]	24.6
Systolic BP, mmHg	146 [28]	133.5 [24]	146 [24.8]	150 [15.25]	153
Diastolic BP, mmHg	80 [5]	82 [4]	78 [3]	83 [7.8]	94
Year of education	14 [6]	13.5 [5.25]	15 [3]	11 [0.75]	10
MoCA	28 [1]	28 [2.5]	28 [1]	25 [3.5]	26
APOE ε4 carrier, *n* (%)	10 (43.5)	4 (50)	3 (33.3)	2 (40)	1 (100)

Abbreviations: SCI, subjective cognitive impairment; MCI, mild cognitive impairment; BMI, body mass index; IQR, inter-quartile range; BP, Blood pressure; MoCA, Montreal Cognitive Assessment, APOE4 = apolipoprotein E4. Group abbreviations: SCI-control, SCI with omega-3- and flavanol-poor intervention; SCI-active, SCI with nutritional (OM3FLAV) intervention; MCI-control, MCI with omega-3- and flavanol-poor intervention; MCI-active, MCI with omega-3- and flavanol-rich intervention.

[a] Values are given as median [IQR] unless stated otherwise.

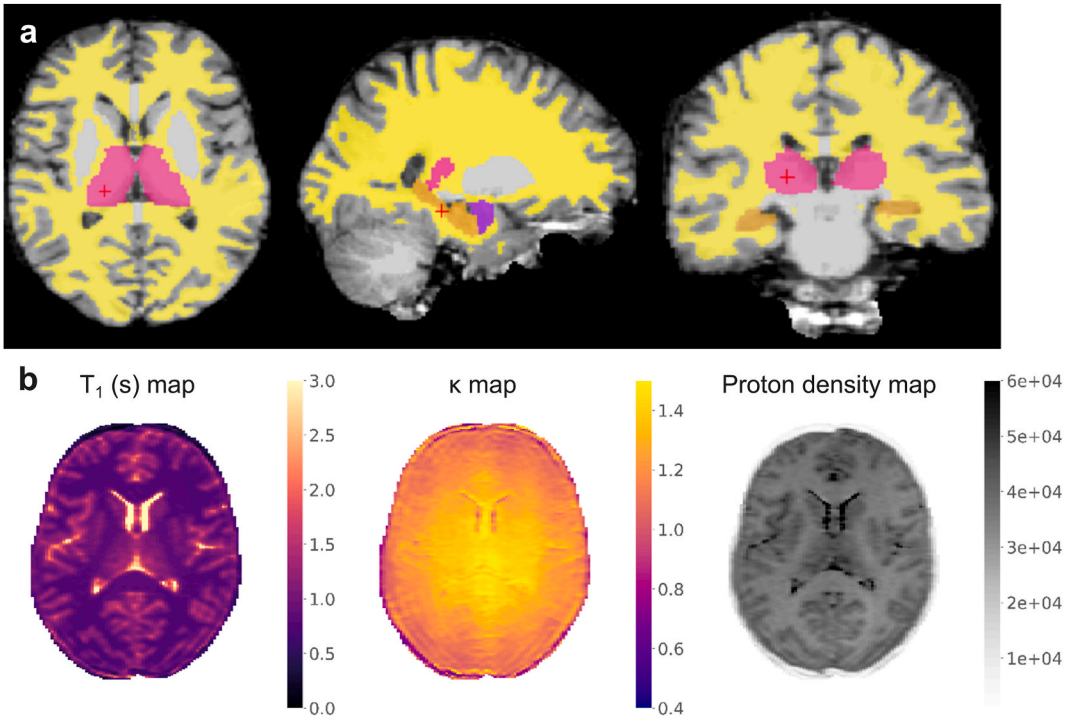

Fig. 1. (a): FreeSurfer segmentation results for a 58-year-old female subjective cognitive impairment (SCI) participant after 12 months taking an omega-3 fatty acid and flavanol (OM3FLAV) intervention. Region of interest colors: yellow, white matter; orange, hippocampus; purple, amygdala; magenta, thalamus. (b) native T_1, relative flip angle (κ), and proton density maps for the same subject.

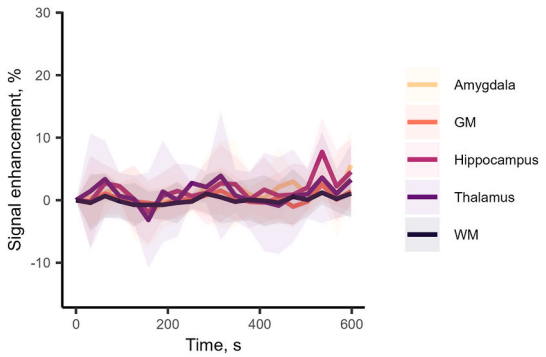

Fig. 2. Median drift in signal enhancement from 3D multi-phase SPGR sequence (identical to DCE-MR, without contrast injection). Scanner drift for each region of interest (ROI) was calculated as the slope of the linear fit to the normalized (non-contrast) signal-intensity-versus-time curves. Ribbons show the interquartile range at each timepoint over all participants. Drifts for all regions showed a small, positive trend, but were within the limits established in previous studies [43].

also tended to be higher for some ROIs, such as the hippocampus and thalamus; however, none of these reached statistical significance. The parcellation volumes and cortical thicknesses were not different for any regions of the brain. These data are provided in the supplementary results: SUPP1a, 1b, and 1c provide parcellation volumes for the MCI-c, SCI-a, and SCI-c groups, respectively. SUPP2a, 2b, and 2c provide cortical thickness for the left hemisphere and SUPP3a, 3b, and 3c provide those for the right hemisphere for the MCI-c, SCI-a, and SCI-c groups, respectively.

3.5. *Merged SCI and MCI groups showed differences in leakage and T_1 values*

After observing no significant effect of the intervention on the SCI cohort, we combined the SCI and MCI control and active groups, including the single MCI-active participant, to determine whether the full SCI cohort (SCI-a+c) showed any difference in DCE-parameters to the MCI cohort (MCI-a+c) for each region. The results show that the plasma volume (v_p) for the combined SCI

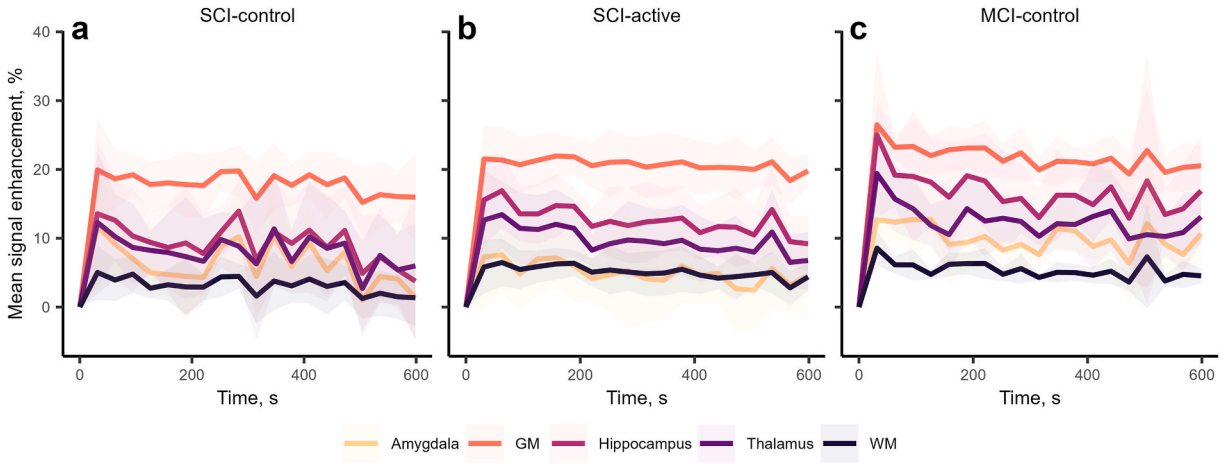

Fig. 3. Average signal enhancement curves for multiple regions of interest (ROIs) in the subjective cognitive impairment (SCI) control group (panel a; n = 8), SCI active group (panel b; n = 9), and mild cognitive impairment (MCI) control group (panel c; n = 5). Median signal enhancement curves for each ROI were measured and averaged over all subjects in the group to obtain these signal enhancement versus time data. Ribbons show the standard deviation per timepoint over all participants in each group. The signal enhancement curves for the single MCI-active group participant are not shown.

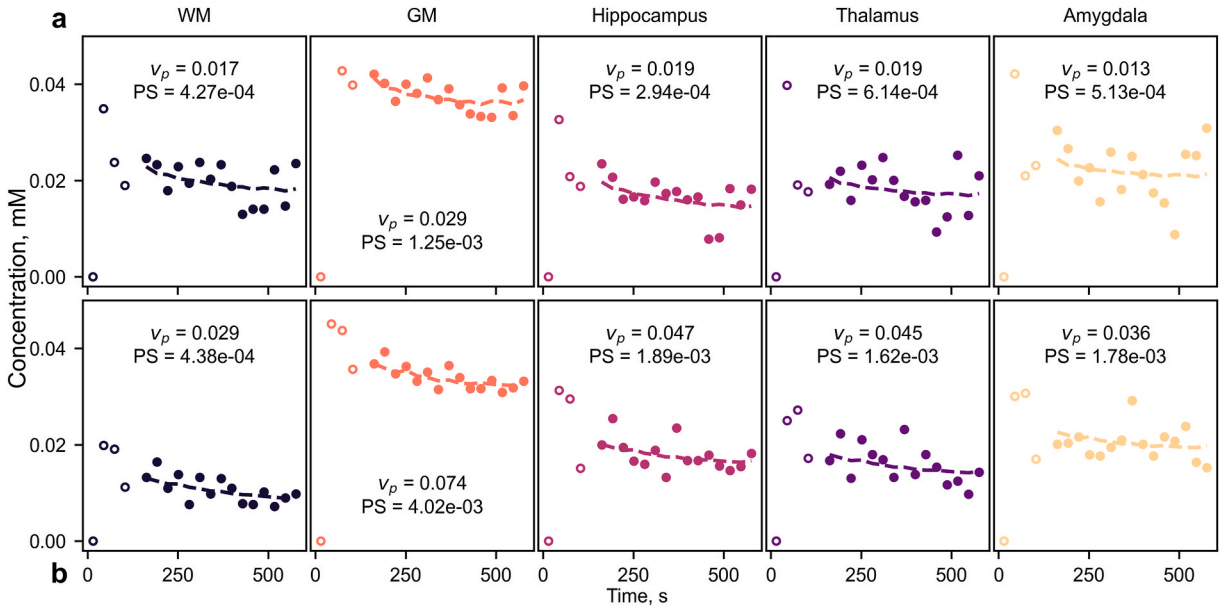

Fig. 4. Patlak model fits (dashed lines) for each concentration time curve (circles) of the analysed ROIs for: (a) 58-year-old female participant with subjective cognitive impairment in the active group (SCI-a). (b) 58-year-old female participant with mild cognitive impairment in the control group (MCI-c). For each region, the blood plasma volume v_p is given along with the permeability surface area product PS. The first four time-points, which are excluded from fitting, are represented by open circles.

cohort was not significantly different to that of the combined MCI cohort. However, the leakage (PS) for the hippocampus and thalamus were significantly higher for the combined-MCI group (MCI-a+c) ($p = 0.019$ and 0.042, respectively) as compared to the combined-SCI cohort (SCI-a+c), with median (IQR) = 1.13 (0.99) versus 0.42 (0.57) $\times 10^{-3}$ min^{-1} for the hippocampus and 0.93 (1.12) versus 0.41 (1.02) $\times 10^{-3}$ min^{-1} for the thalamus. For the amygdala, leakage in the combined-MCI group tended to be greater ($p = 0.06$) as compared to the combined-SCI group, with a median (IQR) PS = 0.61 (0.88) $\times 10^{-3}$ min^{-1} versus 0.07 (1.23) $\times 10^{-3}$ min^{-1}.

The longitudinal relaxation time constant, T_1, was also significantly higher in the MCI cohort than in the combined-SCI cohort for the WM and thalamus ($p = 0.042$ and 0.023, respectively), with median (IQR) = 0.77 (0.054) s and 0.96 (0.063) s, respectively. For the hippocampus, the T_1 in the combined-MCI cohort tended to be higher ($p = 0.06$), with a median (IQR) of 1.20 (0.06) s, as compared to

Table 2
Median with inter-quartile range (IQR) for blood plasma volume (v_p), permeability surface area product (PS) and pre-contrast longitudinal relaxation time constant (T_1) for different regions of interest (ROIs) in the three groups. The single participant in the MCI-active group is included for reference.

ROI	v_p, $\times 10^{-2}$				PS, $\times 10^{-3}$ min^{-1}				Native T_1, s			
	SC-c ($n = 8$)	SC-a ($n = 9$)	MC-c ($n = 5$)	MC-a ($n = 1$)	SC-c ($n = 8$)	SC-a ($n = 9$)	MC-c ($n = 5$)	MC-a ($n = 1$)	SC-c ($n = 8$)	SC-a ($n = 9$)	MC-c ($n = 5$)	MC-a ($n = 1$)
WM	0.94 (0.40)	1.46 (0.07)	1.22 (1.35)	1.24	−0.05 (1.17)	0.32 (0.66)	0.44 (0.42)	0.11	0.76 (0.05)	0.77 (0.05)	0.81 (0.05)	0.76
GM	2.88 (1.00)	2.74 (0.95)	2.63 (3.04)	3.4	1.41 (0.79)	1.51 (0.60)	1.81 (1.01)	0.15	1.17 (0.10)	1.17 (0.12)	1.17 (0.09)	1.13
Hippocampus	1.55 (1.00)	1.68 (0.32)	1.80 (1.28)	2.1	0.4 (1.38)	0.56 (0.56)	1.20 (0.90)	0.04	1.16 (0.05)	1.2 (0.08)	1.2 (0.08)	1.12
Thalamus	1.45 (1.20)	1.89 (0.77)	2.13 (1.53)	1.8	0.06 (1.33)	0.44 (0.48)	1.24 (1.38)	−0.06	0.96 (0.07)	0.96 (0.06)	1.02 (0.04)	0.94
Amygdala	1.15 (0.30)	1.07 (0.78)	1.41 (1.03)	2.1	0.34 (1.24)	−0.04 (1.23)	0.79 (0.96)	−0.06	1.22 (0.15)	1.22 (0.09)	1.28 (0.06)	1.21

Group abbreviations: SC-c, subjective cognitive impairment (SCI) with omega-3- and flavanol-poor intervention; SC-a, SCI with nutritional (OM3FLAV) intervention; MC-c, mild cognitive impairment (MCI) with omega-3- and flavanol-poor intervention; MC-a, MCI with nutritional (OM3FLAV) intervention.
Note: Higher values of PS suggest greater BBB leakage; lower T_1 values can suggest certain pathologies, e.g. endothelial failure, infiltration of solid substance, decrease in water content.

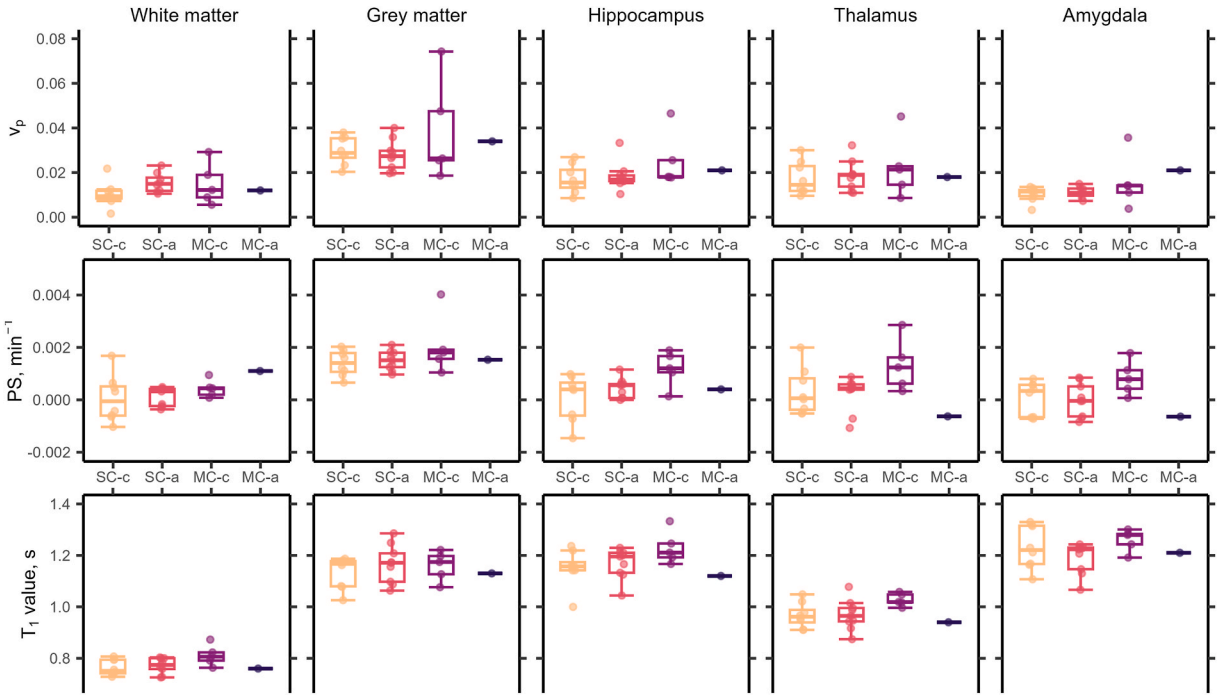

Fig. 5. Boxplots of fractional plasma volume (v_p; panel a), permeability surface area product (PS; panel b), and T_1 (panel c) in larger regions of interest (ROIs): white matter (WM) and grey matter (GM) and in subcortical ROIs: hippocampus, thalamus, and amygdala for different groups, as obtained after 12 months of intervention. Higher PS represents higher leakage, thus lower BBB integrity; higher T_1 indicates general loss of tissue integrity. No significant differences were observed between any of the groups. The MCI-a group (n = 1) is shown here for completeness and was excluded from statistical analysis at this stage. Group abbreviations: SC-c, subjective cognitive (impairment) (SCI) with omega-3- and flavanol-poor intervention; SC-a, SC(I) with nutritional (OM3FLAV) intervention; MC-c, mild cognitive (impairment) (MCI) with omega-3- and flavanol-poor intervention; MC-a, MC(I) with omega-3- and flavanol (OM3FLAV) intervention (n = 1).

1.16 (0.07) s in the combined-SCI group.

4. Discussion

In this pilot sub-study of the CANN trial, we investigated local differences in BBB permeability, for the first time, in approximately age- and BMI-matched SCI and MCI cohorts—two groups demonstrating early indications of higher life-time dementia or Alzheimer's disease risk. We also investigated the effect of a *combined* oral OM3FLAV intervention comprising cocoa flavan-3-ols and long chain omega-3 fatty acids on microvascular integrity and brain structure for the SCI cohort. It should be noted that our primary focus was to explore whether there exists any difference in BBB leakage and T_1 between SCI and MCI participants, rather than to perform a large-scale investigation of the impact of the dietary intervention on these parameters. This choice was motivated by the results of the parent CANN study, which found no differential effect of the intervention on the SCI and MCI groups [22,23]. Indeed, we observed no significant impact of OM3FLAV on BBB leakage in the SCI group [26].

When comparing SCI and MCI subgroups, comprising active and control intervention arms, we saw no differences in BBB leakage, T_1, cortical thickness or parcellation volume, possibly due to limited statistical power. Given that both the original CANN study and this pilot sub-study did not find any significant impact of the combined dietary intervention, we elected to merge the intervention subgroups (i.e. active and control) into larger groups and compare v_p, PS, and T_1 between these SCI and MCI groups. We found significant increases in the regional leakage and T_1 values in the full MCI cohort compared to the SCI group. The observed PS difference likely reflects lower BBB integrity in MCI, which is further supported by the T_1 increase indicating general loss of tissue integrity, possibly due to myelin or axonal loss [44].Our brain volumetric analyses showed no differences in parcellation volume and cortical thickness between groups, indicating that any T_1 differences cannot be attributed to cerebral atrophy. For the MCI group, we observed elevated leakage and T_1 values in the thalamus, amygdala and hippocampus, which represent major components of the limbic system and are specifically involved in memory processing—consistent with the memory-related complaints of MCI participants. For larger ROIs, the T_1 and PS increases may be masked due to the inclusion of functionally spared or diverse regions.

Multiple published works have reported higher leakage in MCI [2,45–47], in participants with 'very mild' dementia symptoms [48], or in *APOE* ε4 carriers [47,49], as compared to healthy controls. We observed an elevated PS in our MCI cohort as compared to SCI. Indeed, the leakage parameters obtained in this study are congruent with values reported in the literature. For example, Ha et al. reported similar range of leakage for multiple brain regions in a cognitively-normal older population (mean age 64.5 years) using both

automated and manual segmentation [31]. Montagne et al. reported slightly higher median leakage in the hippocampus compared to our study, with an arterial input function (AIF) detected from the common carotid artery and using a modified Patlak analysis [8]. However, for participants whose ages matched those of our study, the leakage values are comparable. For the SCI cohort, the reported PS and v_p values agree with those obtained by Lee et al., with a similar age-range of participants [9]. It should be noted that there is substantial variation in DCE-MRI metrics in the literature [10],due to methodological variation in the image acquisition, scanner manufacturer and model, analysis, AIF/VIF location, and so on. Indeed, DCE-MRI parameters are influenced by noise, gross motion, motion artefacts, and *k*-space sampling [50]. PS, in particular, shows a negative bias and increased variance due to these effects, which may explain the presence of non-physiological negative PS values in our results [50], although we observed no gross motion or artefacts in our data. Further, v_p and PS are likely to scale according to the Fåhræus effect, due to a different apparent hematocrit in capillaries in smaller brain regions [51]. Given the difficulty in measuring or modelling such effects from participant to participant, this remains a limitation of the DCE-MRI method. Finally, variation in the results can also be due to different disease stages, small sample sizes, study design, physical activity of the cohort, geographic location, or dietary habits. Therefore, any comparisons with DCE-MRI findings reported in the literature should be undertaken with care, considering these aspects.

Our pre-contrast T_1 values also agree well with the literature. The median T_1 values for WM and GM agree well with the expected range for 3T, (WM: 0.83, GM: 1.31 s) [52–55]. For subcortical regions, our T_1 values were lower than those previously reported in healthy subjects. Lee et al. for example, reported T_1 values of 1.70 s and 1.82 s for the hippocampus and amygdala, respectively [53,55]—values much higher than those observed in larger ROIs. The lower T_1 values in our cohort could be due to the underlying pathology; for example, endothelial failure, infiltration of protein, amyloid β, or inflammatory cells [1]. This, in turn, increases solid deposits and/or decreases the water content. Minor differences in T_1 values may also arise from cohort demographics, the underlying T_1-mapping technique used, or scanner hardware or software. However, we expect that our T_1 estimates are more accurate, as we accounted for B_1^+ inhomogeneity by including ROI-wise map of relative FA as a fitting parameter using the DESPOT1-HIFI method [28,38]. For the thalamus, the T_1 values also agreed well with those reported in literature (0.95—1.03 s) [56,57].

The CANN study explored the *combined* effect of OM3FLAV, as the individual molecular targets of omega-3 fatty acids and flavonoids suggest a synergistic effect [26]. DHA uniquely provides the fatty acid 'building blocks' for cell membrane synthesis associated with increased neurogenesis and synaptic signal transmission [58,59]. Flavan-3-ols are anti-inflammatory; they reduce the production of the neurotoxic Aβ40-42 peptides and promote neuronal survival, neurogenesis, synaptic plasticity, dendritic spine formation and the production of brain derived neurotrophic factor (BDNF) [60,61]. Moreover, a more recent study exploring the positive effect of chronic cranberry consumption (rich in flavonoids) on episodic memory and regional brain perfusion provides a retrospective justification for this co-administration study [62]. As mentioned previously, the parent CANN study found no effect of the combined intervention on cognitive domain or brain structure. Vauzour et al. [26], acknowledge that the one-year intervention duration may not be sufficient to realize any neurophysiological changes associated with enrichment of brain membranes with DHA, given its long half-life of 2.5 years [63]. Further, differentiation of subtle BBB changes in SCI or MCI from typical healthy aging, or from a dietary intervention, demands a highly-sensitive MRI protocol, and sufficiently large active and control intervention groups, perhaps in a crossover design. This pilot work represents the first step towards such studies.

To explore the differences in BBB leakage for SCI and MCI groups, we implemented advanced DCE-MRI analysis as per recent consensus recommendations [10]. Here, we quantified voxel-wise relative FA, native T_1, and proton density using the DESPOT1-HIFI method before performing pharmacokinetic modelling. Accounting for B_1^+ inhomogeneity in this way serves to increase the accuracy of low-level leakage measurement [28,37]. Importantly, we also performed signal drift quantification as part of this work. When present, drift can add significant uncertainty or bias in PS measurements—masking the change in dynamic concentration or limiting the ability of the analysis to detect subtle leakage [64]. Moreover, the permeability parameters extracted from the Patlak model are sensitive to drift—even more so for conditions yielding low-level leakage [28,64], which is exactly the case for this study. As drift is scanner- or subject-dependent, the absence of correction could account for the large variability in leakage values across the literature—which covers three orders of magnitude, including negative values [28]. In this study, we found drift to be either comparable or below the values reported by Cramer et al. at 3T (0.07-0.20% per minute) [65], Heye et al. at 1.5T (0.06−0.1 per minute) [28], and Manning et al. (close to zero at 3T) [37]. It was also within the limit suggested by a multi-center survey of fMRI quality assurance (0.15% per minute) [66]. DCE-MRI in general is subject to pitfalls and challenges [67], being of relatively low sensitivity and requiring the use of GBCAs, some of which are known to accumulate in the brain [68]. Recent work has demonstrated applications of non-contrast arterial spin labeling MRI methods for measuring BBB permeability in ageing and Alzheimer's disease [69,70]. These methods use water as an endogenous tracer, which—given that it has a lower molecular weight than GBCAs—could provide an alternative assessment of BBB dysfunction in the early stages of dementia, albeit with limited spatial information as compared to DCE-MRI [71].

Although permeability in several brain regions was investigated, we did not examine cerebral perfusion. This is because the slower injection used in this study results in a less-perfusion-sensitive DCE-MRI protocol and similar arterial, capillary, and venous concentration curves. Along with slow injection of GBCA, four data points were excluded during model fitting to improve accuracy and decrease systematic errors [37]. We chose to exclude 124 s worth of time series data, which falls between the exclusion ranges used in the recent study of Manning et al. (119 s) and the earlier research of Heye et al. (292 s) [28,37]. These exclusions also serve to mitigate the effect of dispersion on the VIF which is more pronounced in the period immediately after injection. However, this approach reduces sensitivity to perfusion and therefore perfusion-related parameters were not extracted.

Given the preliminary nature of this work, there are some limitations. We recruited relatively small groups of participants, which limited our statistical power, and the group sizes were also different. We included participants from the CANN trial's UK arm subsequent to double-blind randomization, and thus had no control over the ultimate makeup of our placebo and active groups. The MCI group might be expected to benefit most from the intervention; however, due to the aforementioned double-blind randomization, we

were only able to include one MCI-active subject, and so could not explore this hypothesis. In future development of this study, we aim to collect longitudinal data to assess the change from baseline within and across groups. A lack of healthy controls also limited our ability to compare the leakage and T_1 parameters of the SCI and MCI groups to a healthy population. Our DCE-MRI acquisition lasted 10.5 min, whereas. longer scan times (15-20 min) have been shown to increase the reproducibility of DCE-MRI measurements [10,72]; however, practicalities like increased costs, scanner availability, and participant discomfort and resulting motion limited the feasibility of longer scans. To add to that, essential pre-DCE-MRI scans (DESPOT1-HIFI and high resolution T_1-weighted imaging) add extra time to the protocol. Future studies should aim to reduce the total scan duration by interleaving scans [10], for example. Finally, the manual VIF selection process adds a degree of subjectivity to our study; future work should explore automatic VIF detection for increasing objectivity and reproducibility.

5. Conclusions

In this pilot study, we showed for the first time that advanced DCE-MRI analysis techniques can be applied to quantify and compare microvascular integrity in MCI and in its earlier subjectively-defined stage, SCI. Also, we investigated the combined effect of a one-year-long omega-3 fatty acid and flavonoid-based intervention on BBB leakage and brain volumes. Although larger brain regions did not show any difference in leakage between SCI and MCI groups, we observed significantly higher BBB leakage and longitudinal relaxation time constants in brain regions associated with memory in MCI as compared to SCI participants. This confirms the anticipated increased leakage of the BBB in individuals with MCI. Although the results of this preliminary study did not show any significant effect of the OM3FLAV intervention on the SCI cohort, the trends observed in leakage and relaxation time indicate that larger trials with more participants and longer scan durations could be more definitive on the inter- and intra-cohort effects of the dietary intervention on BBB integrity.

CRediT authorship contribution statement

Rashed Sobhan: Writing – original draft, Visualization, Software, Methodology, Investigation, Formal analysis, Conceptualization. **Michael J. Thrippleton:** Writing – review & editing, Supervision, Software, Conceptualization. **David R. Willis:** Software, Methodology, Investigation, Formal analysis, Conceptualization. **Rachel Gillings:** Resources, Project administration. **Saber Sami:** Writing – review & editing, Conceptualization. **Joanna M. Wardlaw:** Writing – review & editing, Supervision, Conceptualization. **Anne-Marie Minihane:** Writing – review & editing, Supervision, Resources, Project administration, Conceptualization. **Narelle M. Berry:** Supervision, Resources, Project administration, Investigation, Funding acquisition, Conceptualization. **Donnie Cameron:** Writing – review & editing, Supervision, Software, Methodology, Investigation, Conceptualization.

Availability of data and materials

The data that support the findings of this study are available from the corresponding author upon reasonable request.

Ethics approval and consent to participate

Ethical approval was granted by the National Research Ethics Service Committee, East of England – Norfolk (Study ID: 14/EE/0189) on the July 16, 2014. Each participant received a comprehensive description of the study, including possible risks, and gave written informed consent prior to participation.

Declaration of competing interest

The authors declare the following financial interests/personal relationships which may be considered as potential competing interests: Narelle Berry reports financial support was provided by Rank Prize. If there are other authors, they declare that they have no known competing financial interests or personal relationships that could have appeared to influence the work reported in this paper.

Acknowledgements

This research was supported by seed funding from Norwich Research Park, and a Rank Prize Funds Nutrition Committee New Lecturer Award, granted to Dr Narelle Berry. This paper is dedicated to the memory of Narelle, our friend and colleague, who passed away in July 2019. For the present work, we would like to thank radiographers Richard Greenwood, Jenna Green, and Neil Saunders for their assistance with setting up the study and scanning participants, and our University of East Anglia IT colleague Dr Jacob Newman for helping to set up the necessary software on our high-performance cluster and supporting our computational analyses.

Appendix A. Supplementary data

Supplementary data to this article can be found online at https://doi.org/10.1016/j.heliyon.2026.e44621.

References

[1] H.J.v.d. Haar, et al., Blood-brain barrier leakage in patients with early alzheimer disease, Radiology 281 (2) (2016) 527–535.
[2] A.K. Heye, et al., Assessment of blood–brain barrier disruption using dynamic contrast-enhanced MRI. A systematic review, Neuroimage, Clin. 6 (2014) 262–274.
[3] Á. Nyúl-Tóth, et al., Linking peripheral atherosclerosis to blood-brain barrier disruption: elucidating its role as a manifestation of cerebral small vessel disease in vascular cognitive impairment, GeroScience 46 (6) (2024) 6511–6536.
[4] Á. Nyúl-Tóth, et al., Demonstration of age-related blood-brain barrier disruption and cerebromicrovascular rarefaction in mice by longitudinal intravital two-photon microscopy and optical coherence tomography, Am. J. Physiol. Heart Circ. Physiol. 320 (4) (2021) H1370–h1392.
[5] R. Gulej, et al., Endothelial deficiency of insulin-like growth factor-1 receptor leads to blood-brain barrier disruption and accelerated endothelial senescence in mice, mimicking aspects of the brain aging phenotype, Microcirculation 31 (2) (2024) e12840.
[6] M. Prince, et al., The global prevalence of dementia: a systematic review and metaanalysis, Alzheimer's Dement. 9 (1) (2013) 63–75.e2.
[7] R. Brookmeyer, S. Gray, C. Kawas, Projections of Alzheimer's disease in the United States and the public health impact of delaying disease onset, Am. J. Publ. Health 88 (9) (1998) 1337–1342.
[8] A. Montagne, et al., Blood-brain barrier breakdown in the aging human hippocampus, Neuron 85 (2) (2015) 296–302.
[9] W.J. Lee, et al., Cognitive improvement effect of gintonin might be associated with blood-brain barrier permeability enhancement: dynamic contrast-enhanced MRI pilot study, Transl Clin Pharmacol 29 (1) (2021) 21–32.
[10] M.J. Thrippleton, et al., Quantifying blood-brain barrier leakage in small vessel disease: review and consensus recommendations, Alzheimer's Dement. 15 (6) (2019) 840–858.
[11] X. Wang, et al., Neuroimaging advances regarding subjective cognitive decline in preclinical Alzheimer's disease, Mol. Neurodegener. 15 (1) (2020) 55.
[12] G. Desideri, et al., Benefits in cognitive function, blood pressure, and insulin resistance through cocoa flavanol consumption in elderly subjects with mild cognitive impairment: the Cocoa, Cognition, and Aging (CoCoA) study, Hypertension 60 (3) (2012) 794–801.
[13] E.E. Devore, et al., Dietary intakes of berries and flavonoids in relation to cognitive decline, Ann. Neurol. 72 (1) (2012) 135–143.
[14] C. Boudrault, R.P. Bazinet, D.W. Ma, Experimental models and mechanisms underlying the protective effects of n-3 polyunsaturated fatty acids in Alzheimer's disease, J. Nutr. Biochem. 20 (1) (2009) 1–10.
[15] P.A. Jackson, et al., DHA-rich oil modulates the cerebral haemodynamic response to cognitive tasks in healthy young adults: a near IR spectroscopy pilot study, Br. J. Nutr. 107 (8) (2012) 1093–1098.
[16] P.A. Jackson, et al., Docosahexaenoic acid-rich fish oil modulates the cerebral hemodynamic response to cognitive tasks in healthy young adults, Biol. Psychol. 89 (1) (2012) 183–190.
[17] O.M. Shannon, et al., Mediterranean diet adherence is associated with lower dementia risk, independent of genetic predisposition: findings from the UK Biobank prospective cohort study, BMC Med. 21 (1) (2023) 81.
[18] M.C. Morris, et al., Consumption of fish and n-3 fatty acids and risk of incident Alzheimer disease, Arch. Neurol. 60 (7) (2003) 940–946.
[19] M.A. Beydoun, et al., Plasma n−3 fatty acids and the risk of cognitive decline in older adults: the Atherosclerosis risk in communities Study2, Am. J. Clin. Nutr. 85 (4) (2007) 1103–1111.
[20] C. Dullemeijer, et al., n−3 fatty acid proportions in plasma and cognitive performance in older adults2, Am. J. Clin. Nutr. 86 (5) (2007) 1479–1485.
[21] E.J. Schaefer, et al., Plasma phosphatidylcholine docosahexaenoic acid content and risk of dementia and Alzheimer disease: the framingham heart study, Arch. Neurol. 63 (11) (2006) 1545–1550.
[22] E. Corradini, et al., Flavonoids: chemical properties and analytical methodologies of identification and quantitation in foods and plants, Nat. Prod. Res. 25 (5) (2011) 469–495.
[23] L. Letenneur, et al., Flavonoid intake and cognitive decline over a 10-year period, Am. J. Epidemiol. 165 (12) (2007) 1364–1371.
[24] R. Krikorian, et al., Blueberry supplementation improves memory in older adults, J. Agric. Food Chem. 58 (7) (2010) 3996–4000.
[25] M.A. Irvine, et al., The cognitive ageing, nutrition and neurogenesis (CANN) trial: design and progress, Alzheimer's Dement.: Translational Research & Clinical Interventions 4 (1) (2018) 591–601.
[26] D. Vauzour, et al., A combined DHA-Rich fish oil and cocoa flavanols intervention does not improve cognition or brain structure in older adults with memory complaints: results from the CANN randomized, controlled parallel-design study, Am. J. Clin. Nutr. (2023).
[27] S.P. Sourbron, D.L. Buckley, Tracer kinetic modelling in MRI: estimating perfusion and capillary permeability, Phys. Med. Biol. 57 (2) (2012) R1–R33.
[28] A.K. Heye, et al., Tracer kinetic modelling for DCE-MRI quantification of subtle blood-brain barrier permeability, Neuroimage 125 (2016) 446–455.
[29] P.A. Armitage, et al., Use of dynamic contrast-enhanced MRI to measure subtle blood–brain barrier abnormalities, Magn. Reson. Imaging 29 (3) (2011) 305–314.
[30] S. Taheri, et al., Blood-brain barrier permeability abnormalities in vascular cognitive impairment, Stroke 42 (8) (2011) 2158–2163.
[31] I.H. Ha, et al., Regional differences in blood-brain barrier permeability in cognitively normal elderly subjects: a dynamic contrast-enhanced MRI-based study, Korean J. Radiol. 22 (7) (2021) 1152–1162.
[32] I.C.M. Verheggen, et al., Increase in blood-brain barrier leakage in healthy, older adults, GeroScience 42 (4) (2020) 1183–1193.
[33] M.S. Albert, et al., The diagnosis of mild cognitive impairment due to Alzheimer's disease: recommendations from the National Institute on Aging-Alzheimer's Association workgroups on diagnostic guidelines for Alzheimer's disease, Alzheimer's Dementia 7 (3) (2011) 270–279.
[34] M. Jenkinson, et al., Improved optimization for the robust and accurate linear registration and motion correction of brain images, Neuroimage 17 (2) (2002) 825–841.
[35] S.M. Smith, Fast robust automated brain extraction, Hum. Brain Mapp. 17 (3) (2002) 143–155.
[36] M. Jenkinson, S. Smith, A global optimisation method for robust affine registration of brain images, Med. Image Anal. 5 (2) (2001) 143–156.
[37] C. Manning, et al., Sources of systematic error in DCE-MRI estimation of low-level blood-brain barrier leakage, Magn. Reson. Med. (2021).
[38] S.C. Deoni, High-resolution T1 mapping of the brain at 3T with driven equilibrium single pulse observation of T1 with high-speed incorporation of RF field inhomogeneities (DESPOT1-HIFI), J. Magn. Reson. Imag. 26 (4) (2007) 1106–1111.
[39] R. Deichmann, et al., Optimization of 3-D MP-RAGE sequences for structural brain imaging, Neuroimage 12 (1) (2000) 112–127.
[40] A.D. Elster, Gradient-echo MR imaging: techniques and acronyms, Radiology 186 (1) (1993) 1–8.
[41] M. Rohrer, et al., Comparison of magnetic properties of MRI contrast media solutions at different magnetic field strengths, Investig. Radiol. 40 (11) (2005) 715–724.
[42] H.B. Larsson, et al., Measurement of brain perfusion, blood volume, and blood-brain barrier permeability, using dynamic contrast-enhanced T(1)-weighted MRI at 3 tesla, Magn. Reson. Med. 62 (5) (2009) 1270–1281.
[43] P. Armitage, et al., Extracting and visualizing physiological parameters using dynamic contrast-enhanced magnetic resonance imaging of the breast, Med. Image Anal. 9 (4) (2005) 315–329.
[44] A. Hagiwara, et al., Age-Related Changes in Relaxation Times, Proton Density, Myelin, and Tissue Volumes in Adult Brain Analyzed by 2-Dimensional Quantitative Synthetic Magnetic Resonance Imaging, Investigative Radiology, 2020.
[45] M. Li, et al., Increase of blood-brain barrier leakage is related to cognitive decline in vascular mild cognitive impairment, BMC Neurol. 21 (1) (2021) 159.
[46] D. Kerkhofs, et al., Blood-brain barrier leakage at baseline and cognitive decline in cerebral small vessel disease: a 2-year follow-up study, GeroScience 43 (4) (2021) 1643–1652.
[47] W.J. Moon, et al., Hippocampal blood-brain barrier permeability is related to the APOE4 mutation status of elderly individuals without dementia, J. Cerebr. Blood Flow Metabol. 41 (6) (2021) 1351–1361.
[48] D.A. Nation, et al., Blood-brain barrier breakdown is an early biomarker of human cognitive dysfunction, Nat Med 25 (2) (2019) 270–276.
[49] A. Montagne, et al., APOE4 leads to blood-brain barrier dysfunction predicting cognitive decline, Nature 581 (7806) (2020) 71–76.

[50] J. Bernal, et al., A four-dimensional computational model of dynamic contrast-enhanced magnetic resonance imaging measurement of subtle blood-brain barrier leakage, Neuroimage 230 (2021) 117786.
[51] H.L. Goldsmith, G.R. Cokelet, P. Gaehtgens, Robin Fåhraeus: evolution of his concepts in cardiovascular physiology, Am. J. Physiol. 257 (3 Pt 2) (1989) H1005–H1015.
[52] J.P. Wansapura, et al., NMR relaxation times in the human brain at 3.0 tesla, J. Magn. Reson. Imag. 9 (4) (1999) 531–538.
[53] C. Lee, E.H. Baker, D.M. Thomasson, Normal Regional T1 and T2 Relaxation Times of the Brain at 3T, 2006.
[54] S.C. Deoni, T.M. Peters, B.K. Rutt, High-resolution T1 and T2 mapping of the brain in a clinically acceptable time with DESPOT1 and DESPOT2, Magn. Reson. Med. 53 (1) (2005) 237–241.
[55] N. Gelman, et al., Interregional variation of longitudinal relaxation rates in human brain at 3.0 T: relation to estimated iron and water contents, Magn. Reson. Med. 45 (1) (2001) 71–79.
[56] S.J. Müller, et al., First clinical application of a novel T1 mapping of the whole brain, NeuroRadiol. J. 35 (6) (2022) 684–691.
[57] C. Thaler, et al., T1 relaxation times in the cortex and thalamus are associated with working memory and information processing speed in patients with multiple sclerosis, Front. Neurol. 12 (2021).
[58] T. Oster, T. Pillot, Docosahexaenoic acid and synaptic protection in Alzheimer's disease mice, Biochim. Biophys. Acta 1801 (8) (2010) 791–798.
[59] T. Oster, T. Pillot, Docosahexaenoic acid and synaptic protection in Alzheimer's disease mice, Biochim. Biophys. Acta 1801 (8) (2010) 791–798.
[60] C.M. Williams, et al., Blueberry-induced changes in spatial working memory correlate with changes in hippocampal CREB phosphorylation and brain-derived neurotrophic factor (BDNF) levels, Free Radic. Biol. Med. 45 (3) (2008) 295–305.
[61] R.J. Williams, J.P. Spencer, Flavonoids, cognition, and dementia: actions, mechanisms, and potential therapeutic utility for Alzheimer disease, Free Radic. Biol. Med. 52 (1) (2012) 35–45.
[62] E. Flanagan, et al., Chronic consumption of cranberries (Vaccinium macrocarpon) for 12 weeks improves episodic memory and regional brain perfusion in healthy older adults: a randomised, Placebo-Controlled, parallel-groups feasibility Study, Front. Nutr. 9 (2022) 849902.
[63] J.C. Umhau, et al., Imaging incorporation of circulating docosahexaenoic acid into the human brain using positron emission tomography, J. Lipid Res. 50 (7) (2009) 1259–1268.
[64] S.R. Barnes, et al., Optimal acquisition and modeling parameters for accurate assessment of low Ktrans blood-brain barrier permeability using dynamic contrast-enhanced MRI, Magn. Reson. Med. 75 (5) (2016) 1967–1977.
[65] S.P. Cramer, H.B. Larsson, Accurate determination of blood-brain barrier permeability using dynamic contrast-enhanced T1-weighted MRI: a simulation and in vivo study on healthy subjects and multiple sclerosis patients, J. Cerebr. Blood Flow Metabol. 34 (10) (2014) 1655–1665.
[66] L. Friedman, G.H. Glover, Report on a multicenter fMRI quality assurance protocol, J. Magn. Reson. Imag. 23 (6) (2006) 827–839.
[67] A. Montagne, et al., Imaging subtle leaks in the blood-brain barrier in the aging human brain: potential pitfalls, challenges, and possible solutions, GeroScience 44 (3) (2022) 1339–1351.
[68] A. Montagne, A.W. Toga, B.V. Zlokovic, Blood-Brain barrier permeability and gadolinium: benefits and potential pitfalls in research, JAMA Neurol. 73 (1) (2016) 13–14.
[69] C. Pappas, et al., Synergistic effects of plasma S100B and MRI measures of cerebrovascular disease on cognition in older adults, GeroScience (2025).
[70] G. Chen, et al., Decreased water exchange rate across the blood-brain barrier throughout the Alzheimer's disease continuum: evidence from Chinese data, Alzheimer's Dement. 21 (3) (2025) e70089.
[71] X. Shao, et al., Comparison between blood-brain barrier water exchange rate and permeability to gadolinium-based contrast agent in an elderly cohort, Front. Neurosci. 14 (2020), 2020.
[72] S.M. Wong, et al., Measuring subtle leakage of the blood–brain barrier in cerebrovascular disease with DCE-MRI: Test–retest reproducibility and its influencing factors, J. Magn. Reson. Imag. 46 (1) (2017) 159–166.